# Laser Tunnel Ionization from Multiple Orbitals in HCl

H. Akagi,[1,2] T. Otobe,[2] A. Staudte,[1] A. Shiner,[1] F. Turner,[1,3] R. Dörner,[4] D. M. Villeneuve,[1] P. B. Corkum[1]*

Tunneling, one of the most striking manifestations of quantum mechanics, influences the electronic structure of many molecules and solids and is responsible for radioactive decay. Much of the interaction of intense light pulses with matter commences with electrons tunneling from atoms or molecules to the continuum. Until recently, this starting point was assumed to be the highest occupied orbital of a given system. We have now observed tunneling from a lower-lying state in hydrogen chloride (HCl). Analyzing two independent experimental observables allowed us to isolate (via fragment ions), identify (via molecular frame photoelectron angular distributions), and, with the help of ab initio simulations, quantify the contribution of lower-lying orbitals to the total and angle-dependent tunneling current of the molecule. Our results bolster the emerging tenet that the coherent interaction between different orbitals—which can amplify the impact of lower orbitals—must be considered in tunneling processes.

When a particle penetrates a barrier without having the necessary energy, it is said to have tunneled. As a fundamental quantum phenomenon that challenges classical intuition, tunneling has been a testing ground for our understanding of quantum mechanics (*1*). Simultaneously, tunneling is having a tremendous impact on technology through applications such as the scanning tunneling microscope (STM) (*2*). The exponential dependence of the tunneling current on the distance between a surface and an STM tip allows for imaging of atomic-scale structure of the surface. By analogy, tunneling of an electron from a molecule by an intense infrared laser pulse can image the electronic structure of single molecules (*3*). In such a "molecular STM," the exponential decay of the wave function in the barrier means that small variations in the ionization potential have a large influence on the ionization probability. Therefore, in atoms and molecules that are subjected to intense laser pulses, the highest electronic state dominates the tunneling current exponentially.

[1]Joint Laboratory for Attosecond Science, University of Ottawa and National Research Council, 100 Sussex Drive, Ottawa, Ontario K1A 0R6, Canada. [2]Quantum Beam Science Directorate, Japan Atomic Energy Agency, Umemidai, Kizugawa-city, Kyoto 619-0215, Japan. [3]University of Waterloo, 200 University Avenue W., Waterloo, Ontario N2L 3G1, Canada. [4]Institut für Kernphysik, Goethe Universität Frankfurt, D-60438 Frankfurt, Germany.

*To whom correspondence should be addressed. E-mail: paul.corkum@nrc.ca

Recently, there has been mounting evidence to suggest that lower-lying levels contribute to the total tunneling current (*4*–*11*). Most evidence arises from structure in the high harmonic spectrum (*6*–*11*). However, because high harmonic radiation is linked to tunneling only through the intermediate steps of continuum propagation and recombination, the interpretation of high harmonic spectra requires sophisticated theories, making quantitative conclusions difficult (*6*, *12*, *13*). Here, by applying our molecular STM technique to the HCl molecule, we observed a 0.2% contribution to the total tunneling current from an orbital with a 30% greater ionization potential than the highest occupied orbital ($I_0 \sim 1.4 \times 10^{14}$ W/cm$^2$). According to our calculations, such a lower-lying orbital can contribute in excess of 10% to the tunneling probability along the molecular axis under otherwise identical conditions. Thus, our measurements support the finding of McFarland *et al.* (*10*) that tunneling from a lower-lying orbital can dominate the high harmonic spectrum for certain molecular alignments. Our results further imply that attosecond hole dynamics resulting from tunneling will be ubiquitous in atoms and molecules (*11*) as well as in solids (*14*).

We chose HCl as an exemplary system because it offers an opportunity to isolate the tunneling current contribution of the highest occupied molecular orbital (HOMO) from that of the next-highest-energy orbital (HOMO-1) (inset, Fig. 1A). The HOMO of HCl is a lone-pair 3p orbital of the Cl atom aligned perpendicular to the molecular axis, whereas the HOMO-1 accounts for the molecular bond and is formed by the overlap of the 1s orbital of the hydrogen atom and a chlorine 3p orbital along the molecular axis.

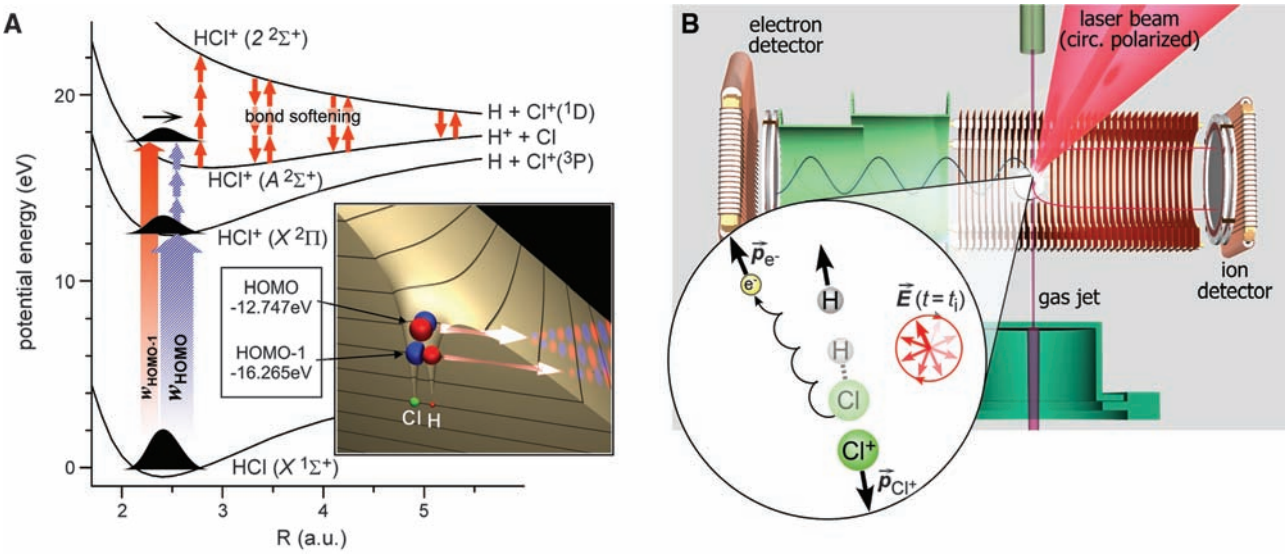


**Fig. 1.** (**A**) Schematic diagram for the tunnel ionization and subsequent bond-softening processes of HCl in an intense near-infrared laser field. Data for the potential energy curves were obtained from (*24*) and (*32*) for ion and neutral states, respectively. The ground state of singly charged $HCl^+$ ion ($X^2\Pi$), produced by ionization from the HOMO of the HCl molecule, does not dissociate in the laser field. In contrast, the first electronic excited state of the $HCl^+$ ion ($A^2\Sigma^+$), produced by ionization from the HOMO-1, dissociates through the bond-softening process by coupling with the $(2)^2\Sigma^+$ state. (**B**) Sketch of electron and fragment ion momenta in the plane of the circularly polarized laser pulse in the present experiment.

Tunneling from the HOMO-1 weakens the bond and, in the laser field, leads to fragmentation of the molecular ion. Hence, the breakup of an HCl molecule after ionization is a direct signature for tunneling from a lower-lying orbital.

Figure 1A illustrates this point using the potential energy surfaces of HCl and $HCl^+$. Here, we consider only ionization to the ground $X^2\Pi$ and first excited $A^2\Sigma^+$ states of the $HCl^+$ ion, as the second excited state of $HCl^+$ requires an additional five photons (i.e., ~7.75 eV). Whereas the ground (X) state is produced by tunnel ionization from the HOMO, the A state has its origin in the HOMO-1. The A state couples strongly with the dissociative $(2)^2\Sigma^+$ state, allowing $HCl^+$ fragmentation through bond softening (*15*). The X state is produced in a transition perpendicular to the molecular axis and does not possess such a direct pathway to dissociation. However, as indicated in Fig. 1A, there is a weak secondary pathway to bond softening (see below).

By measuring the fragment ion and the tunneled electron in coincidence, we determine the molecular frame photoelectron angular distribution (MFPAD) that identifies the HOMO-1 of HCl. The concept, introduced in (*16*), is illustrated in Fig. 1B (*17*). In a cold target recoil ion momentum spectrometer (COLTRIMS) (*18*) an intense, circularly polarized laser pulse singly ionizes and subsequently dissociates an unaligned molecule. The ejected electron drifts perpendicular to the electric field direction at the moment of ionization (*19*); the fragment ion trajectory reflects the orientation of the molecule.

To ensure that only a single electron had tunneled from the molecule and that the fragmentation occurred rapidly enough to preserve the molecular orientation, we needed to establish $HCl^+$ bond softening as the origin of the detected $H^+$ and $Cl^+$ ions. We ruled out a dissociative channel of $HCl^{2+}$ as the origin of the measured fragments because we did not observe a correlation between the $H^+$ and $Cl^+$ momenta. Moreover, the measured kinetic energy spectrum of $H^+$ and $Cl^+$ exhibited discrete peaks. Bond softening often produces multiple peaks in the kinetic energy spectrum of the ion fragments according to the absorbed number of photons (*15*). Finally, we found that $H^+$ and $Cl^+$ ions are emitted within ±30° to ±15° of the polarization plane in the intensity range of $1 \times 10^{14}$ to $2 \times 10^{14}$ W/cm$^2$. A small angular spread is further characteristic of bond softening (*15*).

In Fig. 2, A and B, the kinetic energy spectra of $Cl^+$ and $H^+$ are shown for two intensities: $1 \times 10^{14}$ W/cm$^2$ (dashed line) and $2 \times 10^{14}$ W/cm$^2$ (solid line). The energies of vibrational levels corresponding to the different dissociation pathways are superimposed as vertical lines. Chlorine ions are produced only with a single characteristic kinetic energy in the studied intensity range. As suggested by the vertical lines, the $Cl^+$ energy is consistent with the net-two-photon bond-softening channel, as the dissociation limit of the $H + Cl^+(^1D)$ channel is 2.58 eV above the vibrational ground state of $HCl^+$ ($A^2\Sigma^+$, $v = 0$). Hence, the energy of a laser photon with 1.55 eV is insufficient for net-one-photon dissociation in the $H + Cl^+$ channel. The proton distribution also has a single peak at an intensity of $1 \times 10^{14}$ W/cm$^2$. However, at higher intensity, the hydrogen background in our chamber contributes to the signal. The peak at 100 meV is well known from $H_2^+$ bond softening. Background hydrogen also contributes to the peak at 500 meV. Therefore, in our analysis of protons produced via the $H^+ + Cl$ channel, we only include the net-two-photon peak located near 1.2 eV.

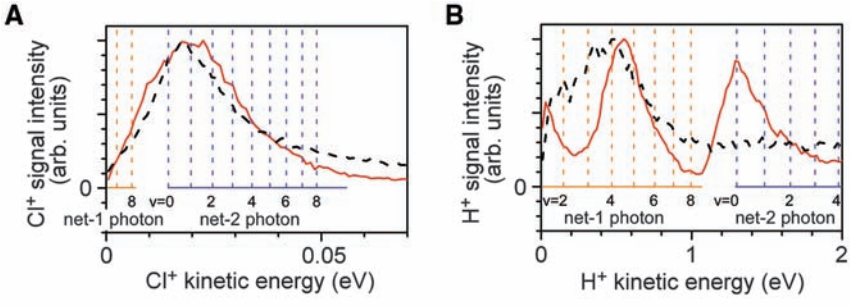


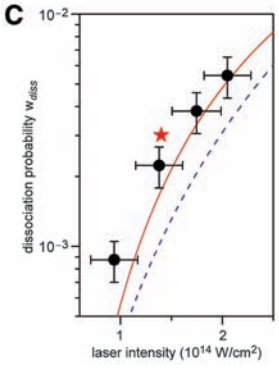


**Fig. 2.** (**A**) $Cl^+$ kinetic energy at $1 \times 10^{14}$ W/cm$^2$ (dashed line) and $2 \times 10^{14}$ W/cm$^2$ (solid line). (**B**) Same as (A) for protons. (**C**) Intensity dependence of the ratio of total yields of the molecular ion $HCl^+$ and the dissociation fragments $H^+$ and $Cl^+$. The error bars in the intensity direction correspond to ±1σ determined by a least-squares fit of electron momentum, whereas the bars in the yield ratio direction indicate ±20% error (*17*). Solid line: $w_{HOMO\text{-}1}/w_{HOMO}$ relative atomic tunneling probabilities for orbitals with the corresponding ionization potential. Star: $w_{HOMO\text{-}1}/w_{HOMO}$ predicted by our molecular DFT calculation. Dashed line: $w_{X\text{-}A}/w_{HOMO}$ relative probability of bond softening from the X state.

Figure 2C shows the laser intensity dependence of the experimentally determined dissociation probability

$$w_{diss} = N_{H^+,{}^{35}Cl^+}/N_{H^{35}Cl^+} \quad (1)$$

where

$$N_{H^+,{}^{35}Cl^+} = [N_{H^+}N_{H^{35}Cl^+}/(N_{H^{35}Cl^+} + N_{H^{37}Cl^+})] + N_{{}^{35}Cl^+} \quad (2)$$

takes the Cl isotope ratio into account for the number of detected protons. The probability to detect dissociated HCl molecules is 9 (±2) × $10^{-4}$ at the lowest intensity of $1 \times 10^{14}$ W/cm$^2$, and increases to 5 (±1) × $10^{-3}$ at the highest intensity experienced by the neutral molecule, $2 \times 10^{14}$ W/cm$^2$.

Using atomic tunneling theory (*20*), we estimate the ionization probabilities $w_{HOMO}$ and $w_{HOMO\text{-}1}$ for the respective equilibrium ionization energies of HOMO (12.747 eV) and HOMO-1 (16.265 eV) (*21*). The calculated ratio $w_{HOMO\text{-}1}/w_{HOMO}$ is shown as the solid curve in Fig. 2C. Within experimental error, the observed ratio coincides with the theory. However, in making this comparison we have assumed that bond softening of the A state is 100% efficient and that the laser field does not alter the excited-state population ratios created by tunneling. For comparison, bond softening in $H_2^+$ dissociates up to 50% of all molecules at similar intensities. Hence, we might expect that the experimentally presented ratio systematically underestimates the total tunneling probability from the lower-lying orbital HOMO-1 by at least a factor of 2. In addition, tunneling theory does not account for other shake-up processes that will contribute (*4*). The ratio determined by a density functional theory (DFT) calculation, described below, is shown as the red star.

We now examine the tunneling probability in the molecular frame. Because tunneling projects a filtered version of the ionizing momentum wave function of the orbital into the continuum (*3*, *20*), the angle-dependent tunneling probability can uniquely differentiate the very different structures of the HOMO and HOMO-1. Figure 3 shows the electron momentum space and the corresponding radially integrated angular distributions when we select electrons that are correlated with either $Cl^+$ (Fig. 3, A and C) or $H^+$ (Fig. 3, B and D) at an intensity of $2 \times 10^{14}$ W/cm$^2$. Both fragmentation channels yield almost identical molecular frame photoelectron angular distributions. Thus, the electron distributions unambiguously identify the HOMO-1 [Fig. 3F, calculated by the full valence CASSCF procedure using the TZV basis sets with polarization functions (*22*)] as the origin of the fragmentation channel.

To quantify the contribution of tunneling from HOMO-1, we compared our experiment to a DFT (*23*) analysis of angular tunneling ionization probability for both HOMO and HOMO-1 in a static field corresponding to an intensity of

$1.4 \times 10^{14}$ W/cm$^2$. Our calculations generally followed the method of (*23*). We found (Fig. 4A) that the theoretical angle-dependent ionization probability follows the basic structure of the orbital as expected. A second important observation from both theory and experiment is that the ionization probability along the molecular axis (θ = 0°, 180°) is asymmetric, although this is not obvious in Fig. 4A because of the dominating asymmetry in the ionization rates parallel to and perpendicular to the molecular axis. For tunneling from the HOMO, our calculation predicts that the probability to ionize from the proton end of the molecule [$w_{HOMO}(\theta = 0°)$] is 1.14 times the probability from the chlorine end of the molecule [$w_{HOMO}(\theta = 180°)$]. For the HOMO-1 this ratio rises to a factor of 1.56, in excellent agreement with the experimental ratio of 1.6 obtained from Fig. 3, C and D, as a ratio of electron yields ejected from the proton end (θ = 0° ± 18°) and from the chlorine end (θ = 180° ± 18°).

The calculated angle-resolved ratio of $w_{HOMO-1}/w_{HOMO}$ (Fig. 4B) suggests that the HOMO-1 contribution can exceed 10% for aligned molecules. Angular integration yields a ratio of $w_{HOMO-1}/w_{HOMO} = 0.6\%$. However, for comparison with our measurement, an alignment factor must be taken into account (*17*), decreasing the ratio to 0.3% (red star in Fig. 2C), in good agreement with the experimental data.

In Fig. 4C the angular tunneling probabilities of the HOMO-1 obtained from experiment and simulation are compared, the theory (solid line) being convoluted with the experimental angular uncertainty (±30°). The measured distributions for all intensities are included. Notably, the experimental data are not intensity dependent. However, there is one major discrepancy with theory: The minimum at 90° is less pronounced in the experiment, and it cannot be accounted for by the experimental resolution alone. We attribute this effect to a contribution from the perpendicular coupling between the ion's ground state and its first excited state through a perpendicular transition (as indicated in Fig. 1A). Using the X-A transition moment matrix theoretically obtained by Pradhan *et al*. (*24*), we estimate the X-A transition fraction of the ion's ground state $w_{X\text{-}A}/w_{HOMO}$ to be 0.1% at an intensity of $1.4 \times 10^{14}$ W/cm$^2$, including the geometrical weight factor of ½ (*17*). The corrected angular distribution (dotted line in Fig. 4C) is in nearly perfect agreement with the experiment.

This experimental asymmetry may be amenable to a qualitative explanation, as follows: The DFT calculation suggests that the main mechanism responsible for the difference in the ionization rate when the field points toward the hydrogen (θ = 0°) versus the chlorine (θ = 180°) atom is the angle-dependent Stark shift of the neutral molecule (*16*). The ground state of the molecule undergoes a Stark shift because of both the permanent and induced dipole moments. In the tunneling limit, the Stark shift adds directly to the ionization potential for the molecule. The ground-state shift is given by

$$\Delta V_g = (\mu_p^g + {}^1/_2\mu_i^g)E \qquad (3)$$

where the induced dipole moment is $\mu_i^g = \alpha E$, determined by the polarizability tensor α and the laser field $E$, and $\mu_p^g$ is the permanent dipole moment of the ground state of the neutral molecule.

A Stark shift of the ion also changes the ionization potential. However, the change in the ionization potential created by the induced dipole in the ion is almost exactly compensated by the modification to the tunneling barrier (*16*, *25*), whereas the ion Stark shift created by the permanent dipole is canceled to ~50% by the modification to the tunneling barrier that it creates. Therefore, the influence of the ion's Stark shift is muted; the neutral molecule plays the dominant role.

On the basis of these considerations, the effective ionization potential $IP_{eff}$ is simply given by

$$IP_{eff}(E) = IP_0 - (\mu_p^g - {}^1/_2\mu_p^i + {}^1/_2\mu_i^g)E \qquad (4)$$

where $\mu_p^i$ is the permanent dipole moment of the A state of the ion. Inserting $IP_{eff}$ into the common quasi-static atomic tunneling equations for linearly polarized light [e.g., equation 7 in (*20*)], we find that the electron is 1.4 times as likely to be ejected when the field points toward the H atom as when the field points toward the Cl atom. This is in qualitative agreement with the experimental asymmetry of 1:1.6.

Our results have broader implications. First, the difference in ionization potential between the HOMO and lower-lying states in larger molecules is generally smaller than the 4 eV of HCl. Therefore, tunneling from two or more orbitals should occur frequently. Depending on how the experiment is performed, these channels can interfere. In our experiment, by measuring the ion, we can distinguish the orbital from which the electron emerged. Like a two-slit experiment where

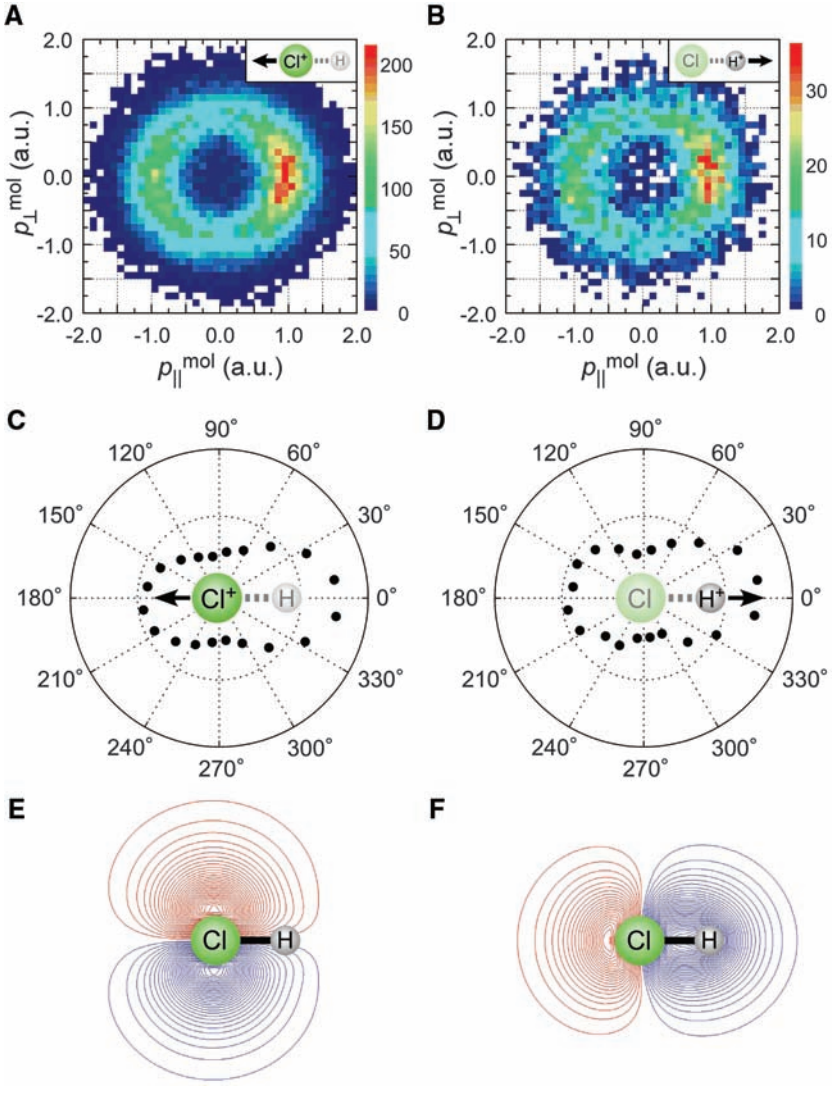


**Fig. 3.** (**A** and **B**) Electron momentum distribution in the molecular frame for the $Cl^+$ and the $H^+$ channels, respectively. (**C** and **D**) MFPADs derived from (A) and (B). Molecules are subjected to a circularly polarized 800-nm laser pulse for 50 fs at a peak intensity of $2 \times 10^{14}$ W/cm$^2$. (**E** and **F**) Two-dimensional representation of the HOMO and HOMO-1 of HCl.

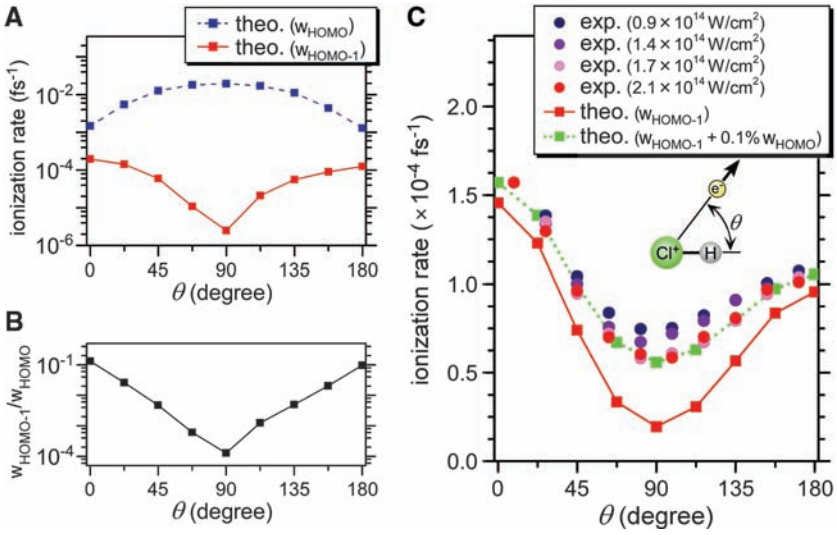


**Fig. 4.** (**A**) DFT calculated angular ionization probability of HOMO [$w_{HOMO}(\theta)$, dashed line] and HOMO-1 [$w_{HOMO-1}(\theta)$, solid line] at an intensity of $1.4 \times 10^{14}$ W/cm$^2$. (**B**) Ratio $w_{HOMO-1}/w_{HOMO}$ from (A). (**C**) Comparison of experiment and theory for the HCl angular ionization probability. The experimental curves are normalized to $\theta = 0°$. Solid line, calculated MFPAD of HOMO-1 convoluted with the experimental angular uncertainty (±30°); dotted line, same as solid line but including 0.1% of the HOMO angular distribution.

we measure the slit through which the electron passes, there can be no interference [except for a post-tunneling shake-up process (*4*) or the weak contribution through the X-A coupling]. However, in many experiments the tunneling orbital is not distinguishable. Electron wave packets must escape through the tunnel within a very restricted time window near each field maximum. Their coherent superposition will influence the angle-dependent rates. This kind of interference may be responsible for the very sharply peaked tunneling distribution found for $CO_2$ (*26*).

Second, ionization creates an electron and a correlated ion (*27*). Simultaneous tunneling from two or more orbitals locks the phase of the ion's states (*11*). Hence, a correlated bound electron wave packet is created in the ion that can be probed by the tunneled electron through recollision. This process is the analog to the creation of vibrational wave packets in molecules by tunneling (*28*, *29*). Whereas vibrational wave packets typically evolve on the femtosecond scale, bound electron wave packets exhibit true attosecond dynamics and are expected to be a ubiquitous feature of laser-driven tunneling in both molecular gases and solids (*14*).

Third, we have shown that tunneling selectively occurs with a specific orientation within a homogeneous sample. The only requirement for probing orbitals (and orbital dynamics) in two-color experiments (*30*, *31*) is that ionization labels the orbital. Our experiment shows that, in principle, molecules could be selected on the basis of their dipole moment.

### References and Notes


1. P. Eckle *et al.*, *Science* **322**, 1525 (2008).
2. G. Binning, H. Rohrer, Ch. Gerber, E. Weibel, *Phys. Rev. Lett.* **49**, 57 (1982).
3. M. Meckel *et al.*, *Science* **320**, 1478 (2008).
4. I. V. Litvinyuk *et al.*, *Phys. Rev. Lett.* **94**, 033003 (2005).
5. W. A. Bryan *et al.*, *Nat. Phys.* **2**, 379 (2006).
6. T. Kanai, S. Minemoto, H. Sakai, *Nature* **435**, 470 (2005).
7. W. Li *et al.*, *Science* **322**, 1207 (2008); published online 29 October 2008 (10.1126/science.1163077).
8. X. Zhou *et al.*, *Phys. Rev. Lett.* **100**, 073902 (2008).
9. W. Boutu *et al.*, *Nat. Phys.* **4**, 545 (2008).
10. B. K. McFarland, J. P. Farrell, P. H. Bucksbaum, M. Gühr, *Science* **322**, 1232 (2008); published online 29 October 2008 (10.1126/science.1162780).
11. O. Smirnova *et al.*, *Nature* 10.1038/nature08253 (2009).
12. Y.J. Chen, J. Liu, B. Hu, *J. Chem. Phys.* **130**, 044311 (2009).
13. A.-T. Le, R. R. Lucchese, M. T. Lee, C. D. Lin, http://arxiv.org/abs/0901.1311 (2009).
14. M. Gertsvolf *et al.*, *Phys. Rev. Lett.* **101**, 243001 (2008).
15. P. H. Bucksbaum, A. Zavriyev, H. G. Muller, D. W. Schumacher, *Phys. Rev. Lett.* **64**, 1883 (1990).
16. A. Staudte *et al.*, *Phys. Rev. Lett.* **102**, 033004 (2009).
17. See supporting material on *Science* Online.
18. J. Ullrich *et al.*, *Rep. Prog. Phys.* **66**, 1463 (2003).
19. P. B. Corkum, N. H. Burnett, F. Brunel, *Phys. Rev. Lett.* **62**, 1259 (1989).
20. N. B. Delone, V. P. Krainov. *Phys. Uspekhi* **41**, 469 (1998).
21. P. Natalis, P. Pennetreau, L. Longton, J. E. Collin, *J. Electron Spectrosc. Relat. Phenom.* **27**, 267 (1982).
22. M. W. Schmidt *et al.*, *J. Comput. Chem.* **14**, 1347 (1993).
23. T. Otobe, K. Yabana, J.-I. Iwata, *Phys. Rev. A* **69**, 053404 (2004).
24. A. D. Pradhan, K. P. Kirby, A. Dalgarno, *J. Chem. Phys.* **95**, 9009 (1991).
25. P. Dietrich, P. B. Corkum, *J. Chem. Phys.* **97**, 3187 (1992).
26. D. Pavicic, K. F. Lee, D. M. Rayner, P. B. Corkum, D. M. Villeneuve, *Phys. Rev. Lett.* **98**, 243001 (2007).
27. H. Niikura *et al.*, *Nature* **417**, 917 (2002).
28. Th. Ergler *et al.*, *Phys. Rev. Lett.* **97**, 103004 (2006).
29. S. Baker *et al.*, *Science* **312**, 424 (2006); published online 1 March 2006 (10.1126/science.1123904).
30. M. Kitzler, M. Lezius, *Phys. Rev. Lett.* **95**, 253001 (2005).
31. D. Shafir, Y. Mairesse, D. M. Villeneuve, P. B. Corkum, N. Dudovich, *Nat. Phys.* **5**, 412 (2009).
32. M. H. Alexander, X. Li, R. Liyanage, R. J. Gordon, *Chem. Phys.* **231**, 331 (1998).



33. Supported by the U.S. Air Force Office of Scientific Research, the Alexander von Humboldt Foundation, the Deutsche Forschungsgemeinschaft, the Canadian Institute for Photonics Innovation, and the Natural Sciences and Engineering Research Council of Canada. We thank B. Avery for technical assistance and M. Zimmer for help in preparing some of the graphics.


### Supporting Online Material

www.sciencemag.org/cgi/content/full/325/5946/1364/DC1
Materials and Methods
Figs. S1 to S3
References


21 April 2009; accepted 9 July 2009
10.1126/science.1175253


# Extremely Efficient Multiple Electron-Hole Pair Generation in Carbon Nanotube Photodiodes


Nathaniel M. Gabor,[1]* Zhaohui Zhong,[2]† Ken Bosnick,[4] Jiwoong Park,[3] Paul L. McEuen[1,2]



We observed highly efficient generation of electron-hole pairs due to impact excitation in single-walled carbon nanotube p-n junction photodiodes. Optical excitation into the second electronic subband $E_{22}$ leads to striking photocurrent steps in the device $I$-$V_{SD}$ characteristics that occur at voltage intervals of the band-gap energy $E_{GAP}/e$. Spatially and spectrally resolved photocurrent combined with temperature-dependent studies suggest that these steps result from efficient generation of multiple electron-hole pairs from a single hot $E_{22}$ carrier. This process is both of fundamental interest and relevant for applications in future ultra-efficient photovoltaic devices.


A single-walled carbon nanotube (SWNT), which can be viewed as a rolled sheet of graphene, generates numerous species of one-dimensional charge carriers whose energies (shown in Fig. 1A) are given by:

$$\varepsilon_i(k) = \pm\sqrt{(m_i^* v_F^2)^2 + (\hbar k v_F)^2} \qquad (1)$$

where $v_F = 8 \times 10^5$ m / s is the Fermi velocity of graphene, $\hbar$ is Planck's constant, $\hbar k$ is the carrier momentum along the length of the nanotube, and $m_i^*$ is the effective mass of the $i$th subband (*1*, *2*). For a semiconducting SWNT, the band-gap energy $E_{11} = 2m_1^* v_F^2$ is the energy required to generate an electron-hole (e-h) pair (Fig. 1B), whereas higher subband energies such as $E_{22} = 2E_{11}$ correspond to excitations with greater effective mass ($m_2^* = 2m_1^*$).

The small Fermi velocity and low dielectric constant in SWNTs suggest that high-energy carriers should efficiently generate e-h pairs. Ef-

# Supporting Online Material for

## Laser Tunnel Ionization from Multiple Orbitals in HCl

H. Akagi, T. Otobe, A. Staudte, A. Shiner, F. Turner, R. Dörner, D. M. Villeneuve, P. B. Corkum*

*To whom correspondence should be addressed. E-mail: paul.corkum@nrc.ca

Published 11 September 2009, *Science* **325**, 1364 (2009)
DOI: 10.1126/science.1175253

**This PDF file includes:**

# Supporting Text A: Experimental Details

Circularly polarized Ti:Sa laser pulses (50-60 fs, 800~nm, up to 9 μJ) were focused with an on-axis parabolic mirror (f = 50 mm) to intensities of (1-4) $x10^{14}$ W/cm$^2$ into a slightly precooled (220 K) supersonic gas jet. The gas jet was produced in a continuous supersonic expansion of 6% HCl diluted in Helium carrier gas with a stagnation pressure of 3 bar through a 30μm nozzle into a vacuum of $<1x10^{-4}$ mBar.

To measure the 3-dimensional momentum vectors of electrons and ions in coincidence we employed Cold Target Recoil Ion Momentum Spectroscopy (COLTRIMS) *(S1)*. Ions and electrons created in the focal region are guided by electric (21 V/cm) and magnetic fields (12 Gauss) towards two micro-channel plate detectors with delay line position encoding *(S2)* on opposite ends of the spectrometer. Positions and time-of-flights were recorded using time-to-digital converters with a resolution of 500 ps *(S3)*. In the analysis we only used the $^{35}Cl^+$ ion signal, because the $^{37}Cl^+$ signal overlapped with the dominant $H^{35}Cl^+$ and $H^{37}Cl^+$ signals.

We expect ±20 % error for the experimentally determined dissociation probability $w_{Diss}$ based on uncertainty of the $^{35}Cl^+$ and $H^+$ ion yields. Because the $^{35}Cl^+$ signal in a direction opposite to the electron detector overlapped with the dominant $H^{35}Cl^+$ signal, we could not determine the ion yield in the direction directly with the experimental data. Hence, the ion yield was evaluated by the yield measured in the other direction, based on the cylindrical symmetry relative to the laser propagation direction. We expect that the evaluation for the $^{35}Cl^+$ yield leads to ±15 % error of $w_{Diss}$, which corresponds to 1/2 of the evaluated yield in the unmeasured direction. On the other hand, $H^+$ signal from $HCl^+$ net-1-photon bond softening was contaminated with $H^+$ ions originated from $H_2$ background in our chamber. Hence, we estimated the fraction from the $HCl^+$ process, comparing the MFPAD with those for $H_2^+$ bond softening *(S4)* and for $HCl^+$ net-2-photon bond softening. We expect ±5 % error caused by the estimation, because the estimated $H^+$ yield corresponds to 10 % of all fragment ions.

While the peak intensity in the focus reached up to $4 \times 10^{14}$ W/cm$^2$ the intensity actually experienced by the HCl molecules is lower due to the saturation of the single ionization. Measuring the magnitude of the radial electron momentum at an intensity well below saturation yielded a calibration of focal intensity with pulse energy *(S5)*. This allows to determine peak intensity in the focus for larger pulse energies. However, in the data analysis we used the intensity determined from the measured electron momentum, because this directly provides the intensity at the time of tunnelling. Non-linear least squares fitting to a theoretical expression of the electron momentum in a circularly polarized laser field *(S6)* was utilized for the intensity determination. As the experimental error of the intensity, we used the standard deviation of the fitting, combined with momentum resolution of the electron detector in our apparatus.

## Supporting Text B: Geometrical Weight Factor for the Ionization Ratio $\omega_{\mathrm{HOMO\text{-}1}}/\omega_{\mathrm{HOMO}}$

The tunnel ionization from the HOMO-1 proceeds mainly in a parallel direction to the HCl molecular axis with a similar angular dependence of $\cos^2\theta$ function [Fig. S1(A)]. This angular dependence indicates that only molecules aligned in a laser field direction can ionize and the fraction of randomly aligned molecules is 1/3 ($=\int_0^{\pi} \cos^2\theta \sin\theta \, d\theta / 2$).

For a circularly polarized light as the present experiment, HCl molecules aligned in the polarization plane can ionize [Figs. S2(A) and (B)], whereas the molecules perpendicular to the polarization plane do not contribute to the ionization [Fig. S2(C)]. Hence, 2/3 of randomly aligned HCl molecules contribute to the ionization.

On the other hand, the ionization from HOMO has $\sin^2\theta$ dependence [Fig. S1(B)], indicating that molecules aligned in a direction perpendicular to a laser field can ionize. Because of two degenerated HOMOs in HCl molecule, 2/3 of randomly aligned molecules can ionize coincidentally. Hence, for a circularly polarized light, HCl

molecules aligned in the polarization plane can ionize from one of HOMOs parallel to the plane [Figs. S3(A) and (C)]. Whereas the molecules perpendicular to the plane can ionize from both the orbitals [Figs. S3(E) and (F)], leading to two times higher rate than the other two molecular alignments. Therefore, we obtain the geometrical weight factor of 1/2 [=(4/3)/(2/3)] for the ratio of $\omega_{HOMO-1}/\omega_{HOMO}$.

## Supporting Text C: Geometrical Weight Factor for the X-A Transition Fraction of $HCl^+$ Ion's Ground State

HCl molecules aligned in a perpendicular direction to the circular polarization plane [Figs. S3(E) and (F)] has two times higher rate of the ionization from the HOMO than the other two molecular alignments [Figs. S3(A) and (C)]. Hence, the $HCl^+$ (X) ions, which can excite to the A state with three-photon absorption, are aligned initially in a perpendicular direction to the polarization plane with 1/2 probability. However, the A state ions aligned in the perpendicular direction cannot dissociate through the bondsoftening because of the dipole direction parallel to the molecular axis (*S7*). Only the A state ions aligned in the polarization plane can dissociate, contributing to the $H^+$ or $Cl^+$ ion signal. The fraction of the A state ions produced from the X-A transition (=1/2) must be taken into account to reproduce the observed angular ionization probability.

### References


S1. J. Ullrich, R. Moshammer, A. Dorn, R. Dörner, L.Ph.H. Schmidt, and H. Schmidt-Böcking. Recoil-ion and electron momentum spectroscopy: reaction-microscopes. *Rep. Prog. Phys.*, **66**,1463, (2003).

S2. Roentdek GmbH, 65779 Kelkheim, Germany, www.roentdek.com.

S3. Cronologic OHG, Am Ulmenrück 7, 60433 Frankfurt, www.cronologic.de

S4. A. Staudte, S. Patchkovskii, D. Pavicic, H. Akagi, O. Smirnova, D. Zeidler, M. Meckel, D.M. Villeneuve, R. Dörner, M.Yu. Ivanov, and P.B. Corkum. *Phys. Rev. Lett.* **102,** 033004 (2009).

S5. A. Alnaser, X. Tong, T. Osipov, S. Voss, C. Maharjan, B. Shan, Z. Chang, and C.L. Cocke, *Phys. Rev. A* **70**, 023413 (2004).

S6. N.B. Delone and V.P. Krainov. *Physics - Uspekhi* **41**, 469 (1998).

S7. P.H. Bucksbaum, A. Zavriyev, H.G. Muller, and D.W. Schumacher, *Phys. Rev. Lett.*, **64**, 1883 (1990).

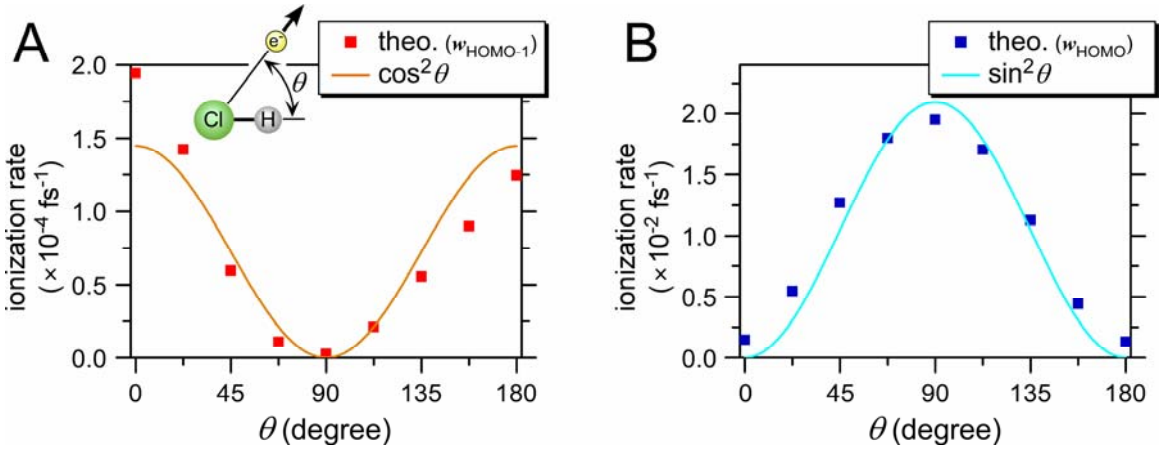


**Fig S1.** (A) Comparison of calculated angular ionization rate of HOMO-1 (solid square) with $\cos^2\theta$ function (solid curve). (B) Comparison of calculated angular ionization rate of HOMO (solid square) with $\sin^2\theta$ function (solid curve).

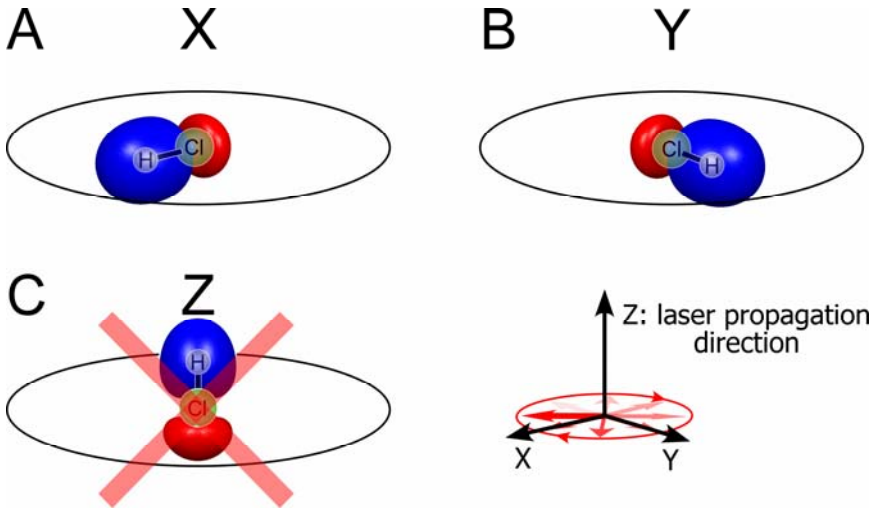


**Fig S2. (A and B)** HOMO-1 in HCl molecules aligned in X and Y directions, respectively. The tunnel ionization from these orbitals proceeds with a laser field rotating in the X-Y plane. **(C)** HOMO-1 in HCl aligned in Z direction. The ionization from the orbital does not proceed.

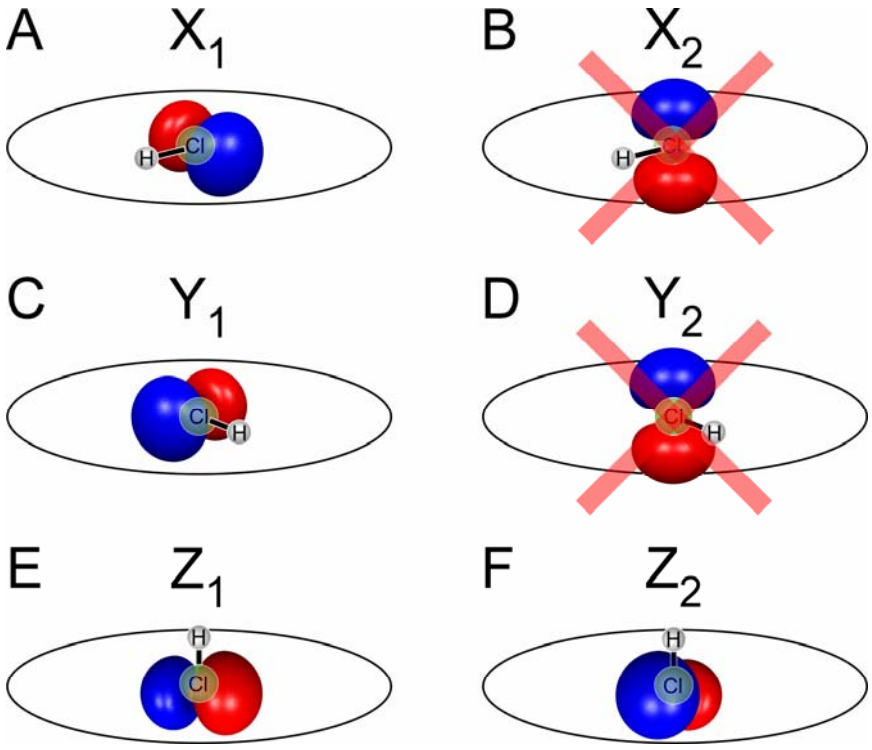


**Fig S3. (A and B)** Two HOMOs in HCl molecule aligned in X direction. For a laser field rotating in the X-Y plane, the ionization proceeds from one of the two orbitals aligned in the polarization plane (A), whereas the other one perpendicular to the plane (B) cannot contribute to the ionization. **(C and D)** Same as (A and B) for HCl molecule aligned in Y direction. **(E and F)** Two HOMOs in HCl molecule aligned in Z direction. Both the orbitals can contribute to the ionization with a laser field rotating in the X-Y plane.